

Sand–rubber mixtures (large rubber chips)

H.-K. Kim and J.C. Santamarina

Abstract: Mixtures of small rigid sand particles D_s and large soft rubber particles D_r are prepared at different volume fractions and tested to investigate their small-strain and zero-lateral strain responses ($D_r/D_s \approx 10$). Both data sets are simultaneously gathered in an oedometer cell instrumented with bender elements. Data are analyzed in the context of mixture theory and with the aid of numerical simulations. Results show that the sand skeleton controls the mixture response when the volume fraction of rubber particles is $V_{\text{rubber}} \leq 0.3$, while the rubber skeleton prevails at $V_{\text{rubber}} \geq 0.6$. The large size and incompressibility of rubber particles provides high stress-induced stiffness in the sand skeleton near the equatorial plane of rubber particles. The corresponding increase in local small-strain shear modulus G_{max} results in earlier wave arrivals in mixtures with $V_{\text{rubber}} \leq 0.3$ than in pure sand, while the quasi-static constrained modulus is highest in pure sand. The constrained modulus and shear wave velocity are power functions of the applied effective stress in all mixtures. Results from this study ($D_r/D_s \approx 10$) and from a previous complementary study with small rubber particles ($D_r/D_s = 0.25$) show that the development of internal fabric, particle level processes, and the associated macroscale response of sand–rubber mixtures depend on the relative size between the soft rubber chips and the stiff sand particles D_r/D_s and their volume fractions.

Key words: recycled tire, wave propagation, constrained modulus, shear wave velocity, granular mixtures.

Résumé : Des mélanges de petites particules rigides de sable D_s et de larges particules molles de caoutchouc D_r ont été préparés à différentes fractions de volume et testés pour étudier leur réaction à de petites contraintes et à déformation latérale nulle ($D_r/D_s \approx 100$). Les deux ensembles de données ont été simultanément regroupées dans une cellule oedométrique instrumentée avec des languettes piézocéramiques. Les données ont été analysées dans le contexte de la théorie du mélange et avec l'aide de simulations numériques. Les résultats montrent que le squelette de sable contrôle la réaction du mélange lorsque la fraction du volume de particules de caoutchouc est $V_{\text{rubber}} \leq 0,3$, alors que le squelette de caoutchouc domine à $V_{\text{rubber}} \geq 0,6$. La grande dimension et l'incompressibilité des particules de caoutchouc fournit une forte rigidité induite par la contrainte dans le squelette de sable près du plan équatorial des particules de caoutchouc. L'accroissement correspondant du G_{max} local résulte en des arrivées plus hâtives des ondes dans les mélanges avec $V_{\text{rubber}} \leq 0,3$ que dans le sable pur, alors que le module quasi-statique sous contrainte est le plus élevé dans le sable pur. Le module sous contrainte et la vitesse des ondes de cisaillement sont des fonctions de puissance de la contrainte effective appliquée dans tous les mélanges. Les résultats de cette étude ($D_r/D_s \approx 10$) et à partir d'une étude complémentaire antérieure avec de petites particules de caoutchouc ($D_r/D_s = 0,25$) montrent que le développement d'une fabrique interne, que les processus de niveau de particules et que la réaction associée à l'échelle macro de mélanges sable-caoutchouc dépendent de la dimension relative entre les fragments mous de caoutchouc et les particules rigides de sable D_r/D_s et leurs fractions de volume.

Mots-clés : pneu recyclé, propagation d'ondes, module sous contrainte, vitesse d'onde de cisaillement, mélanges de grains.

[Traduit par la Rédaction]

Introduction

Granular mixtures can be engineered to exhibit exceptional properties. Early studies of sand–rubber mixtures were prompted by the large number of discarded tires (Edil and Bosscher 1994; Tatlısoz et al. 1997; Rubber Manufacturers Association 2006). Eventually, many construction applications of sand–rubber mixtures, or rubber chips alone, were explored, including highway embankments (Bosscher

et al. 1997; Nightingale and Green 1997; Heimdahl and Druscher 1999), lightweight fill (Ahmed and Lovell 1993; Masad et al. 1996; Lee et al. 1999), backfill for retaining walls (Humphrey and Manion 1992; Humphrey et al. 1993; Garga and O'Shaughnessy 2000), and subsurface drainage systems (Nagasaka et al. 1996).

In general, sand–rubber mixtures exhibit low void ratio, high compressibility, low mass density, high friction angle, and high attenuation (Humphrey et al. 1993; Edil and Bosscher 1994; Foose et al. 1996; Masad et al. 1996; Gebhardt 1997; Wu et al. 1997; Feng and Sutter 2000; Zheng-Yi and Sutter 2000; Yanagida et al. 2002; Yang et al. 2002; Zornberg et al. 2004; Pamukcu and Akbulut 2006).

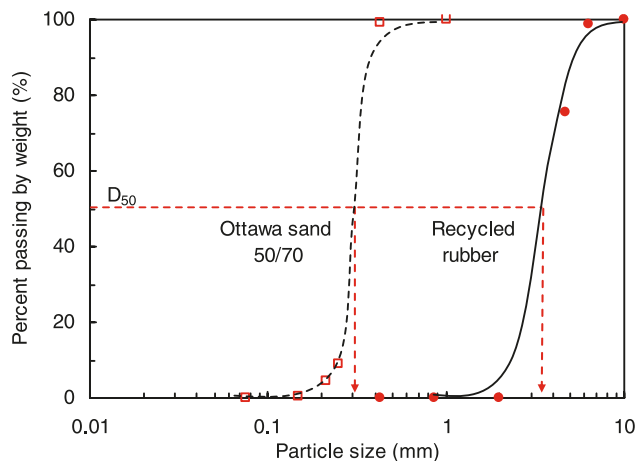
A more detailed examination suggests that the mixture response and underlying sand–rubber interaction mechanisms depend on (i) the volume fraction of the components, and (ii) the ratio between the sand grain size D_s and rubber grain size D_r . Prior studies have explored a range of D_r/D_s values: $D_r/D_s \approx 0.25$ (Lee et al. 2007), $D_r/D_s \approx 0.8$ – 1.1 (Yanagida

Received 29 March 2006. Accepted 25 March 2008. Published on the NRC Research Press Web site at cgj.nrc.ca on 2 October 2008.

H.-K. Kim. Department of Civil and Environmental Engineering, Kookmin University, Seoul, South Korea.
J.C. Santamarina.¹ School of Civil and Environmental Engineering, Georgia Institute of Technology, Atlanta GA 30332, USA.

¹Corresponding author (e-mail: jcs@gatech.edu).

Fig. 1. Particle size distribution of Ottawa 50/70 sand and rubber particles.



et al. 2002; Pamukcu and Akbulut 2006), $D_r/D_s \approx 4$ (Zheng-Yi and Sutter 2000), $D_r/D_s \approx 10$ (Youwai and Bergado 2003; Ghazavi 2004), $D_r/D_s \approx 20$ (Ahmed and Lovell 1993; Masad et al. 1996; Yang et al. 2002), $D_r/D_s \approx 100$ (Humphrey et al. 1993; Lee et al. 1999), and $D_r/D_s \gg 100$ (Edil and Bosscher 1994; Foose et al. 1996; Gebhardt 1997; Zornberg et al. 2004). When the particle size ratio exceeds $D_r/D_s > 6$, size effects are considered to be negligible (Youwai and Bergado 2003).

The purpose of this study is to explore the roles of large soft inclusions $D_r/D_s \approx 10$ in modifying small-strain and zero-lateral strain stiffness of granular mixtures, and to identify underlying particle-level mechanisms at different volume fractions. Then, we compare the behavior of these mixtures ($D_r/D_s \gg 1$) with previously published results for mixtures where $D_r/D_s = 0.25$ (Lee et al. 2007).

Experimental study: materials and devices

Ottawa 50/70 sand (mean grain diameter $D_{50} = 0.35$ mm, specific gravity $G_s = 2.65$) and rubber chips ($D_{50} = 3.5$ mm, $G_s = 1.14$) are used in this study; the particle size ratio is $D_r/D_s \approx 10$. Figure 1 shows the particle size distribution of each material. Rubber particles are angular, while Ottawa sand particles are subrounded. These and other significant differences between sand and rubber particles are summarized in Table 1.

Let us define the volume fraction of rubber particles V_{rubber} as the ratio between the volume of rubber and the total volume of solids. We prepared mixtures at the following volume fractions of rubber particles: $V_{\text{rubber}} = 0.0, 0.1, 0.2, 0.3, 0.4, 0.5, 0.6, 0.7$, and 1.0. Homogeneous mixtures cannot be attained for $V_{\text{rubber}} = 0.8$ or 0.9 because the bulk volume of sand is insufficient to fill the pore space in the rubber skeleton, and sand particles fall by gravity through the porous network (Fig. 2).

Segregation is an inherent difficulty in granular mixtures. In sand–rubber mixtures, segregation is triggered by differences in size, density, stiffness, and shape characteristics. Segregation needs to be considered, especially in mixtures

Table 1. Properties of rubber from pneumatic tires and natural quartz sand.

Used material properties	Recycled rubber	Quartz sand Ottawa 50/70 sand)
Specific gravity	1.14*	2.65
Mean grain diameter, D_{50} (mm)	3.50	0.35
Sphericity	~0.2	0.9 [†]
Roundness	~0.6	0.5 [†]
Maximum void ratio, e_{max}	—	0.85 [‡]
Minimum void ratio, e_{min}	—	0.50 [‡]
Mass density (kN/m^3)	5.98 [§]	15.4
Young's modulus (kPa) [‡]	1020	5.9×10^7
Shear modulus (kPa) [‡]	340	2.4×10^7
Bulk modulus (kPa) [‡]	0.2×10^7	3.7×10^7
Poisson's ratio [‡]	~0.50	0.23

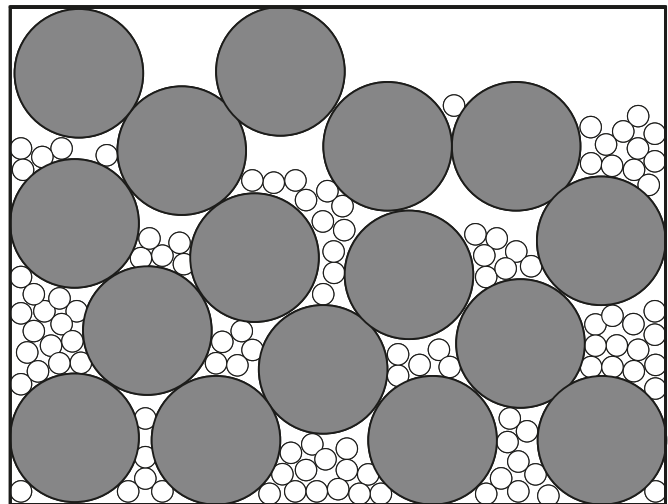
*by ASTM D854.

[†]Data from Lee et al. (2007).

[‡]Data from Walter and Clark (1981).

[§]at $\sigma'_v = 10$ kPa.

Fig. 2. Gravity-biased packing of large and small particles when the volume fraction $V_{\text{large}}/V_{\text{small}} \geq 0.7$. The example shown corresponds to $V_{\text{small}} = 15\%$, $D_r/D_s = 6$.

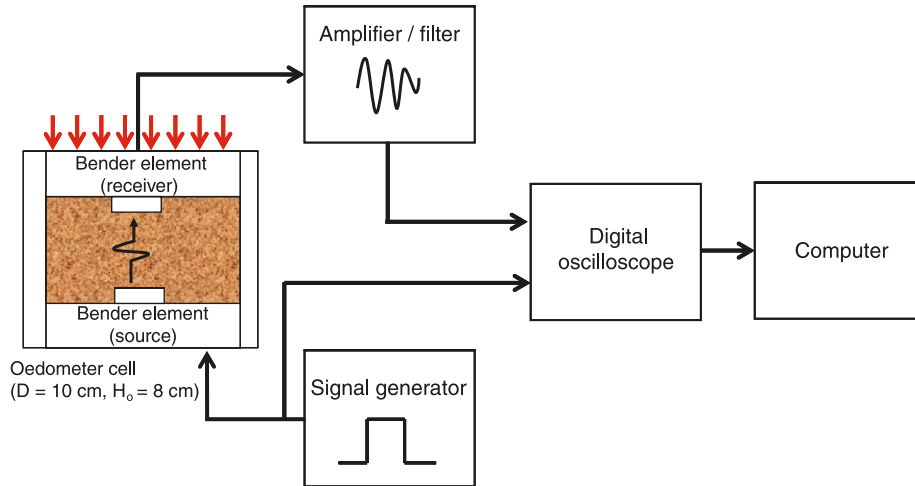


with a large volume fraction of rubber (Edil and Bosscher 1994). We prevented segregation in these specimens by minimizing any vibration and avoiding granular flow during specimen preparation.

Rubber–sand mixtures are tested in a modified oedometer cell (internal diameter 100 mm; specimen height from ~50 mm). The cell is instrumented with bender elements for the simultaneous measurement of shear wave velocity and zero-lateral strain stiffness. Bender elements are mounted on the top cap and the bottom plate of the cell. The input signal fed to the bender element in the bottom plate is a 10 V step signal. Received signals are sampled at 500 kHz. The stacking of 100 signals is used to increase the signal-to-noise ratio before signals are stored in the computer. Figure 3 shows a schematic diagram of the modified oedometer cell and peripheral electronics.

The general test procedure follows that of the conven-

Fig. 3. Schematic diagram of bender element instrumented oedometer cell. D , internal diameter of the cell; H_o , specimen height.



tional consolidation test. The vertical stress is applied in stages: 10, 19, 36, 70, 140, 278, 556, 833, and 1111 kPa; the reverse sequence is followed during unloading. Some mixtures show clear time-dependent deformation. Thus, the final deformation at each loading step is measured when the strain rate becomes negligible, typically within 2 min after load application.

Experimental results

Mixture characteristics, load-deformation response, and stiffness are reported for all tested mixtures in this section.

Mass density

Figures 4a and 4b show measured porosity and mass density versus the volume fraction of rubber particles V_{rubber} . Values are shown at vertical effective stresses of $\sigma'_v = 10$ kPa and 1.1 MPa. In both cases, the minimum porosity is reached at $V_{rubber} \approx 0.6$. The analytical estimation plotted in the same figure is derived under the following assumptions (Youd 1973; Guyon et al. 1987; German 1989): (i) voids between the large rubber particles are large enough to allow for the random packing of small sand particles (note: near-boundary layering affects packing); and (ii) at 10 kPa, rubber particles pack with a void ratio $e_{rubber} = 0.94$ while sand packs with a void ratio $e_{sand} = 0.73$ (experimentally obtained values). The resulting expressions for the porosity, n of mixtures follow:

$$[1] \quad n_{mixture} = \frac{V_{sand}e_{sand}}{1 + V_{sand}e_{sand}} \quad \text{for} \quad V_{sand}e_{sand} \geq (V_{rubber}e_{rubber} - V_{sand})$$

$$[2] \quad n_{mixture} = \frac{V_{rubber}e_{rubber} - V_{sand}}{1 + V_{rubber}e_{rubber} - V_{sand}} \quad \text{for} \quad V_{sand}e_{sand} \leq (V_{rubber}e_{rubber} - V_{sand})$$

These analytical solutions for the porosity of mixtures do not consider the deformation of rubber particles and grain repacking at high pressure. Figure 4c shows the ratio between densities measured at $\sigma'_v = 1.1$ MPa and $\sigma'_v = 10$ kPa

Fig. 4. Gravimetric and volumetric properties of rubber–sand mixtures ($D_r/D_s = 10$). (a) Porosity. (b) Mass density. (c) Mass density ratios at $\sigma'_v = 1.1$ MPa and $\sigma'_v = 10$ kPa. Circles denote measured data; lines are model predictions.

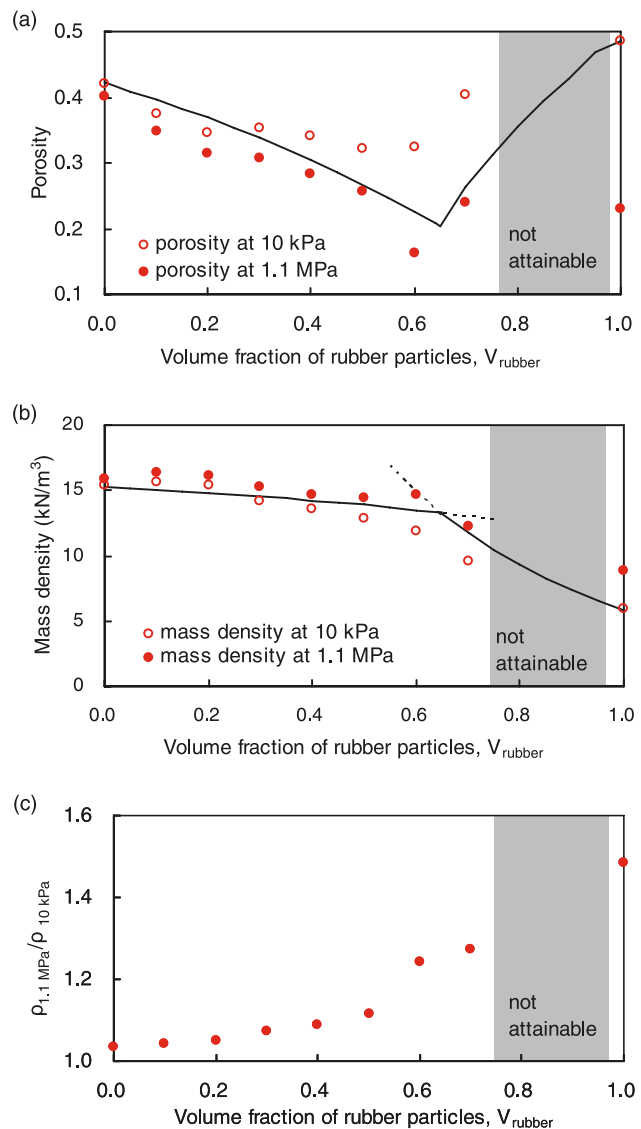
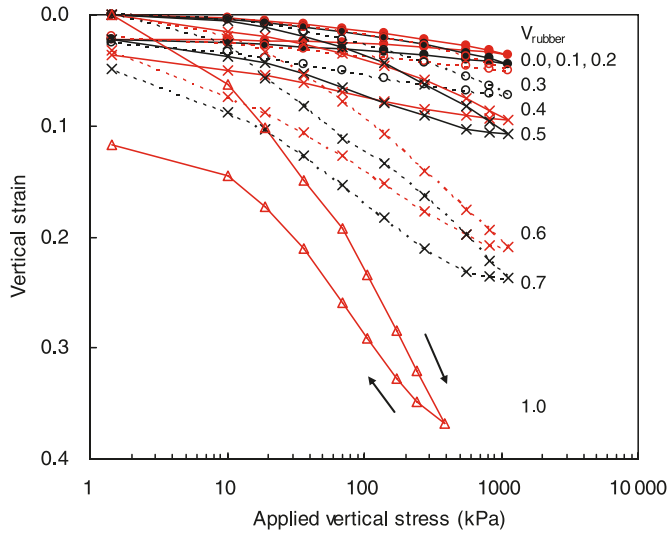


Fig. 5. Zero-lateral strain load-displacement response for different sand–rubber mixtures. Loading and unloading sequences.



versus the volume fraction of rubber particles. The ratio increases significantly when the rubber volume fraction exceeds $V_{rubber} > 0.5$.

Zero-lateral strain compressibility and swell

Figure 5 shows the oedometric stress–strain response for all mixtures. While side friction is expected to lessen deformation (specimen diameter-to-height ratio ≥ 2), trends clearly show increase in compressibility and swell with increasing V_{rubber} . Figure 6a shows the evolution of the constrained modulus, $M = \Delta\sigma_v/\Delta\varepsilon_z$ computed between two successive loading stages during loading for all mixtures. The observed linear trends in log–log scale suggest a semi-empirical power function

$$[3] \quad M = M_1 \left(\frac{\sigma_v}{1 \text{ kPa}} \right)^m$$

where M_1 is the constrained modulus at $\sigma'_v = 1 \text{ kPa}$, and m captures the stress sensitivity of the mixture stiffness. The parameters M_1 and m are plotted against the volume fraction of rubber in Fig. 6b. The data show that when $V_{rubber} \leq 0.2$, the mixture supports the load mainly through the sand skeleton. The increased rubber-to-rubber interaction gradually reduces the effective mixture stiffness as the volume fraction of rubber particles increases, especially when $V_{rubber} \geq 0.5$. When $V_{rubber} \geq 0.6$, most of the applied load is transferred through rubber-to-rubber contacts, and the effective constrained modulus M_1 follows the Ruess lower bound (i.e., harmonic mean), which is very close to the Hashin–Shtrikman lower bound (bounds in Mavko et al. 1998).

Swelling indices, $C_s = -\Delta(\log \sigma'_v)/\Delta\varepsilon_z$ (where ε_z is vertical strain) are computed from $e - \log \sigma'$ data at each unloading stage, and are plotted in Fig. 7. The maximum rebound and C_s values occur at about $\sigma'_v = 100 \text{ kPa}$ for mixtures with $V_{rubber} \geq 0.3$. The underlying mechanism for this peak appears to be related to the evolution of coefficient of earth pressure at rest K_0 in mixtures and the mobilization of wall friction in these specimens.

Fig. 6. Constrained modulus in sand–rubber mixtures. (a) Modulus versus applied vertical stress. (b) Model parameter M_1 and m versus volume fraction of rubber. The ? indicates not attainable.

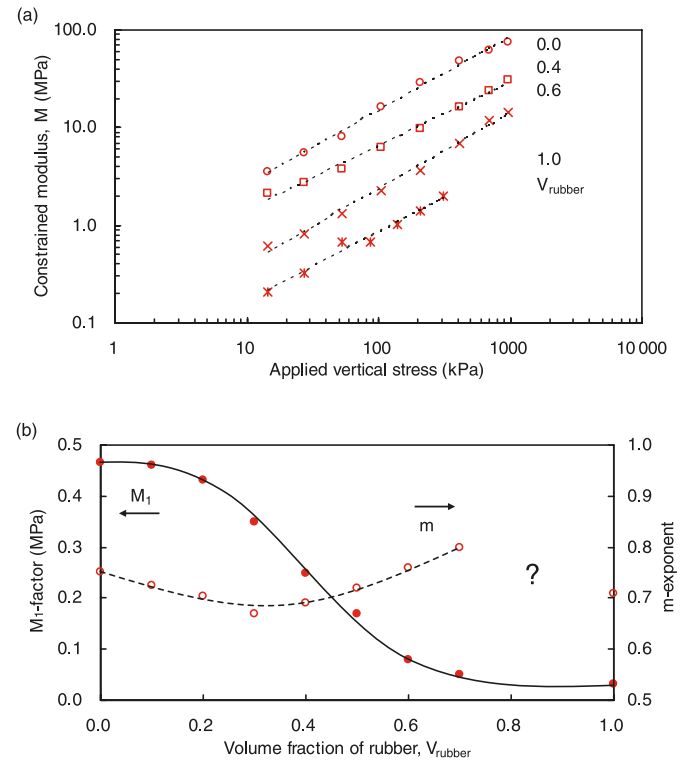
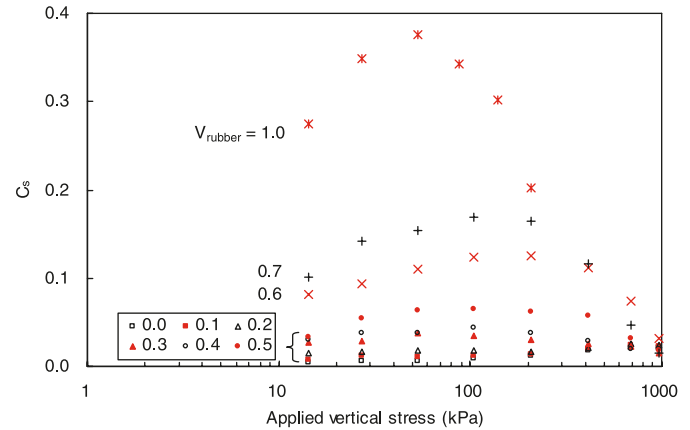


Fig. 7. Swelling index at each unloading stage for all mixtures.



Shear wave velocity

Shear wave signals recorded for the $V_{rubber} = 0.1$ and 0.7 specimens during loading and unloading are shown in Fig. 8. These records highlight the significant differences in material stiffness and stress sensitivity.

Figure 9a shows the evolution in shear-wave velocity with the applied vertical stress for all mixtures during loading. The measured velocities are replotted in Fig. 9b in terms of V_{rubber} . The linear trends in Fig. 9a indicate that the value of V_s can be expressed as a power function of the vertical effective stress σ'_v (note that the mean stress in the polarization plane σ'_o would be more appropriate; Hardin and Black 1968; Knox et al. 1982; Santamarina et al. 2001) as follows:

Fig. 8. Received shear-wave signals during K_0 loading and unloading.

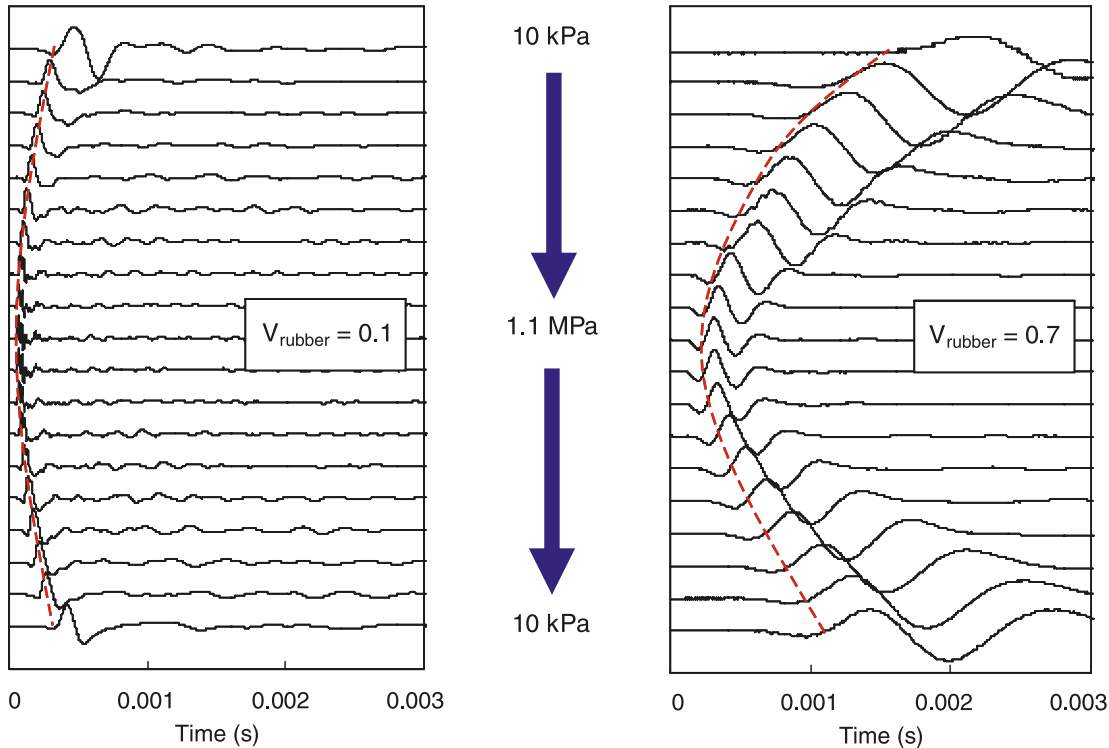
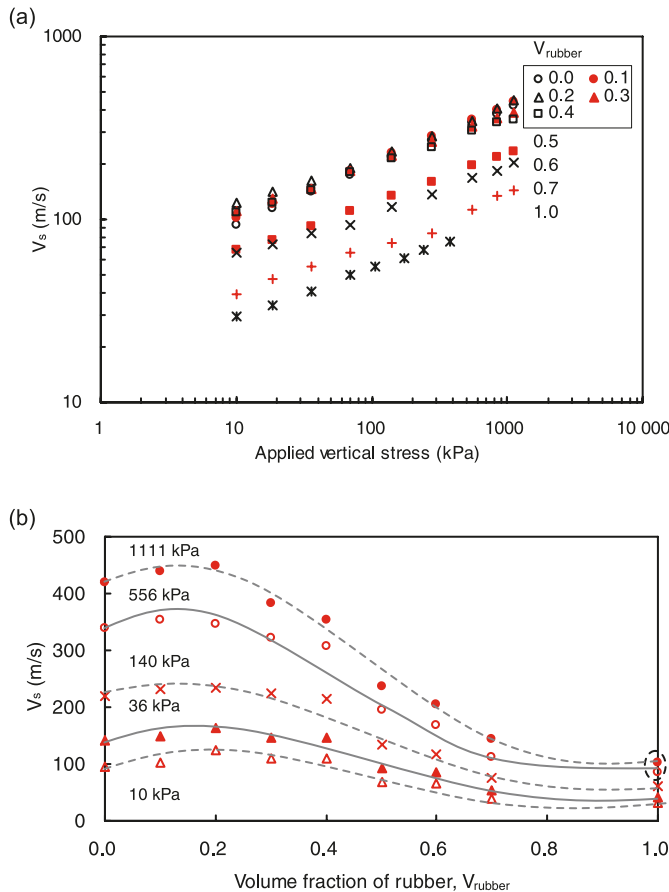


Fig. 9. Shear wave velocity in sand–rubber mixtures. (a) Shear wave velocity versus applied vertical stress. (b) Shear wave velocity versus volume fraction of rubber (encircled values are obtained by extrapolation).



$$[4] \quad V_s = \alpha \left(\frac{\sigma'_v}{1 \text{ kPa}} \right)^\beta$$

where α is the reference shear wave velocity at 1 kPa, and β captures the stress sensitivity of V_s . The α factor and β exponent are plotted against V_{rubber} in Fig. 10. Contrary to the constrained modulus, the shear wave velocity does not decrease monotonically with the volume fraction of rubber. Instead, the maximum shear wave velocity is observed in the $V_{\text{rubber}} = 0.2$ mixture. The shear wave velocity decreases significantly when the rubber volume fraction exceeds $V_{\text{rubber}} > 0.4$. These nonmonotonic trends suggest complex internal interactions. A detailed analysis follows.

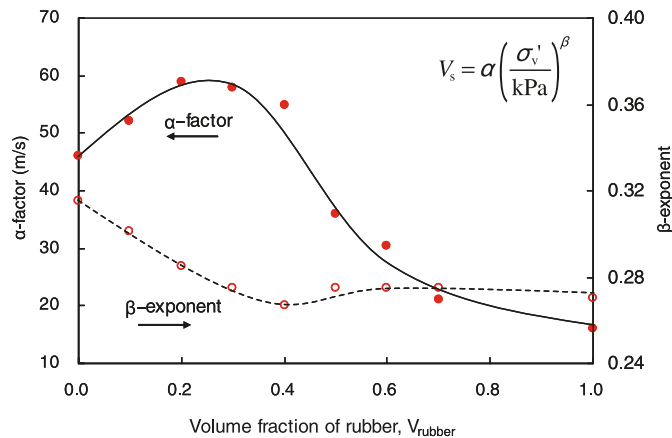
Numerical modeling of sand–rubber mixtures

The experimentally observed nonlinear response of sand–rubber mixtures is further studied through numerical simulations. First, two systems are explored to gain further insight into mixture behavior. Then, sand–rubber mixtures are modeled.

Random mixtures of linear-elastic materials: quasi-static loading

Numerical finite element simulations are conducted to estimate the mechanical behavior of two-phase mixtures of linear elastic materials. The 100×100 four-node element mesh represents a plane-strain slice of a prismatic body. Each element is randomly assigned as either a stiff material (Young’s modulus $E = 1000$ kPa, Poisson’s ratio $\nu = 0.30$) or a soft material ($E = 10$ kPa, $\nu = 0.49$) to satisfy preselected volume fractions. The body is subjected to vertical loading under zero-lateral strain using a rigid cap and bottom plate. Figure 11 shows the normalized effective constrained modulus versus the volume fraction of the soft

Fig. 10. Shear wave velocity model parameters versus volume fraction of rubber.



material V_{soft} . Upper and lower Hashin–Shtrikman’s bounds are shown for reference. The upper bound assumes that the stiff material wraps around the soft material; therefore, the stiff material properties are more important to assess the global mechanical behavior. The opposite is true for the lower bound. The effective constrained modulus determined from the numerical simulations is close to the upper bound when $V_{\text{soft}} \leq 0.3$, but it approaches the lower bound when $V_{\text{soft}} \geq 0.7$.

Nonlinear sand with linear elastic rubber: quasi-static loading

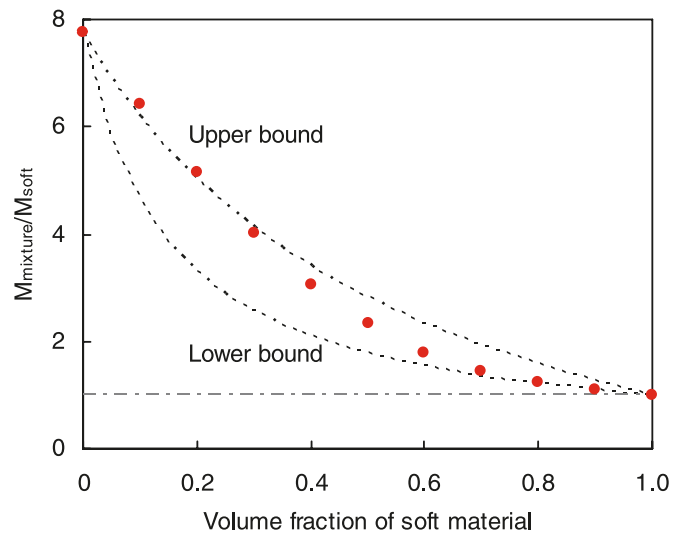
The goal of the next study is to understand the nonlinear interaction between a rubber inclusion and the sand matrix. The sand is modeled as a hypoelastic material by fitting the experimentally measured evolution of the constrained modulus in the oedometer cell: $M = ae^{bz} \approx 8.9e^{63.4z}$ (in MPa and $R^2 = 0.97$). Poisson’s ratio is assumed to be $\nu = 0.2$. On the other hand, rubber is modeled as an isotropic linear elastic material ($E = 1020$ kPa, $\nu = 0.49$; see Table 1).

A four-node 100×100 plane-strain element mesh is used to study the deformation of a single cylindrical rubber particle in the sand–host medium subjected to vertical loading under zero-lateral strain conditions (Fig. 12a). The study is repeated for different sized inclusions $D_{\text{rubber}}/D_{\text{spec}} = 0.36$ ($V_{\text{rubber}} = 0.1$), 0.51 ($V_{\text{rubber}} = 0.2$), and 0.62 ($V_{\text{rubber}} = 0.3$). Results in Fig. 12 show that the soft rubber inclusion promotes vertical and horizontal stress concentration on the equatorial plane around the inclusion. Figure 13 shows measured and predicted $e - \log \sigma'$ results for different mixtures with low V_{rubber} . Note that the numerical simulation presumes no rubber-to-rubber interaction (this assumption loses validity when $V_{\text{rubber}} \geq 0.3$). In these simulations, the equivalent quasi-static constrained modulus decreases monotonically as V_{rubber} increases.

Shear wave propagation in mixtures (short wavelength case)

While the presence of rubber always causes a decrease in the quasi-static constrained modulus, experimental results show that shear waves propagate faster in mixtures $V_{\text{rubber}} \approx 0.2$ than in the pure sand at all stress levels (Fig. 9). Numerical simulations are conducted to identify the underlying

Fig. 11. Effective constrained modulus of random binary linear elastic mixtures. Points represent the numerical prediction and the lines represent the Hashin–Shtrikman bounds.



causal mechanisms. The simulated medium is described in Fig. 14 (mesh similar to Fig. 12a, ABAQUS). A single cylindrical rubber particle is located at the center of the host medium, and a plane shear wave is initiated from the top of the mesh. Short wavelength wave propagation data are gathered for (i) a homogeneous medium without inclusions, (ii) a homogenous elastic host medium with a soft inclusion, and (iii) a host medium with an inclusion, where the local stiffness of the host medium resembles the stress-dependent sand response. In the last case, the local values of the small-strain stiffness are calculated from the previous quasi-static loading simulations with the nonlinear material model (Figs. 12 and 13). The study is conducted to represent the mixture with $V_{\text{rubber}} = 0.2$.

Figure 15 shows time series at different locations. Differences in travel times and shadow effects are clearly seen (typical diffraction healing develops behind the inclusion – Wielandt 1987; Potts and Santamarina 1993). Obviously, travel times in the elastic medium with inclusion are longer than in the homogeneous medium without the inclusion. However, travel times in the stress-dependent medium are shorter outside the shadow area.

Wavelength and propagation modes

The wavelength λ of propagating perturbations must be considered during data analysis. In general, when the wavelength is much greater than the rubber particle size, $\lambda \gg D_r$, the propagation corresponds to an equivalent continuum with stiffness G_{eff} . However, when $\lambda \approx D_r$, propagation must be analyzed as ballistic propagation in heterogeneous media. The central frequency in recorded shear wave signals ranges from $f = 4$ kHz at low confinement ($\sigma'_v = 10$ kPa) to $f = 21$ kHz at high confinement ($\sigma'_v = 1.1$ MPa). The wavelength λ is estimated from velocity V_s and frequency f data $\lambda = V_s/f$. Estimated values range from $\lambda = 7$ mm to $\lambda = 55$ mm, that is $\lambda/D_r = 2\text{--}15$.

Figure 16 shows the ratio λ/D_r computed for the experimental results. The wavelength to size ratio λ/D_r decreases with the increase in the applied stress σ'_v , and it increases

Fig. 12. Numerical simulation of nonlinear sand with a soft elastic inclusion at the center: stress field under 1 MPa K_0 loading condition. Darker areas indicate higher stress.

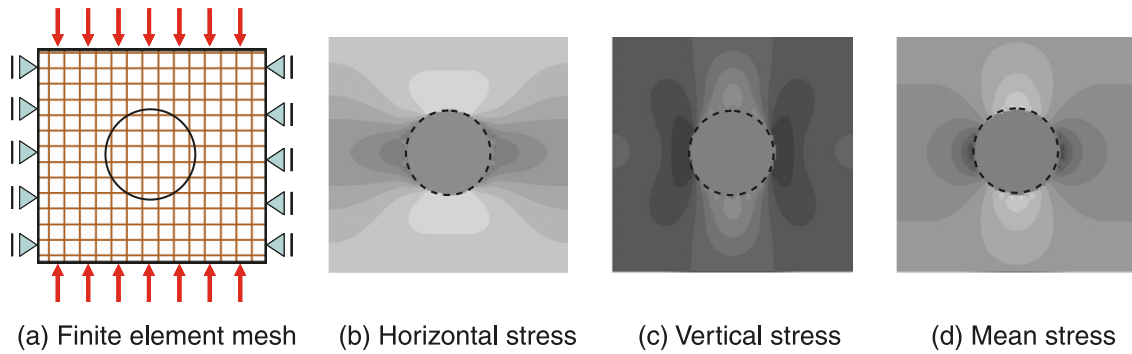
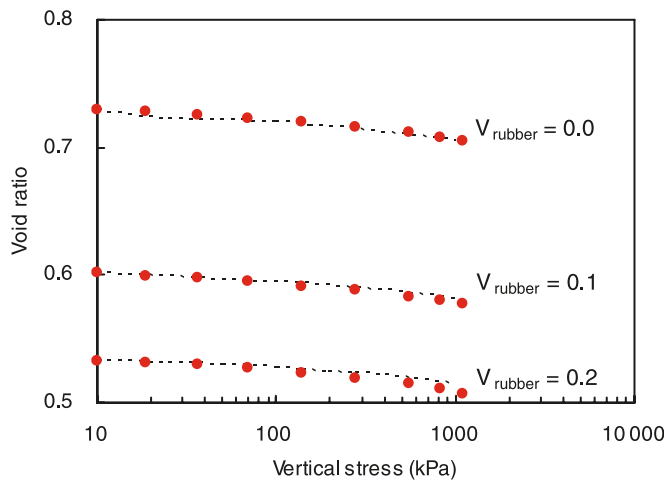


Fig. 13. Load and displacement response comparison for mixtures with small volume fraction of rubber. Nonlinear numerical simulation results (dotted lines) and experimental results (points).



with the increase in the volume fraction of rubber V_{rubber} . The close proximity of rubber particles in mixtures with high V_{rubber} produces a low-pass filtering effect, and only long wavelengths are detected (Brillouin effect; Santamarina et al. 2001).

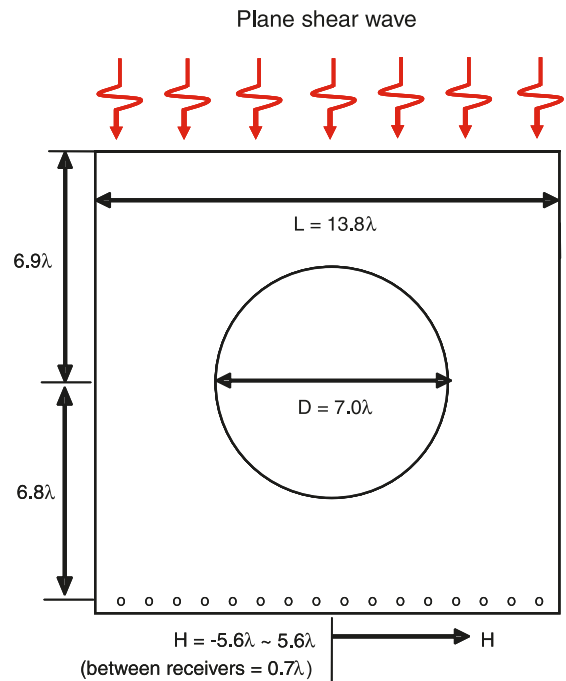
As λ approaches the inter rubber-particle spacing, the travel path becomes tortuous, yet the increase in local stiffness by mean stress concentration ($\sigma'_v + \sigma'_h$) results in faster propagation in mixtures with $V_{rubber} \approx 0.2$ than in pure sand. Eventually, tortuosity prevails in mixtures with higher V_{rubber} .

Discussion: mixtures with small and large D_r/D_s ratios

Figure 17 sketches particle-level phenomena in rubber-sand interaction for particle size ratios $D_r/D_s \gg 1$ and $D_r/D_s \ll 1$, at various volume fractions of rubber V_{rubber} . Distinct fabric, particle level phenomena, and macroscale response are recognized.

In the case of $D_r/D_s < 1$ mixtures, rubber particles tend to fill the voids between sand particles in mixtures with low V_{rubber} , but they eventually separate sand particles as V_{rubber} increases (Lee et al. 2007). Mixtures with intermediate V_{rubber} experience the development of additional sand-to-sand con-

Fig. 14. Numerical simulation of high frequency shear wave propagation in sand-rubber mixture ($V_{rubber} = 0.2$). Infinite boundary elements are used to minimize boundary effects.



tacts as confinement increases, so that these “transition mixtures” behave rubber-like at low confinement and sand-like at high confinement. This transition is confirmed by wave propagation studies (Lee et al. 2007 report the highest value of the b -exponent in $G_{max} = A(\sigma'_v/kPa)^b$ for $V_{rubber} = 0.4$, in $D_r/D_s = 0.25$ mixtures).

In the case of $D_r/D_s \gg 1$ mixtures, rubber particles float within the sand skeleton in mixtures with low V_{rubber} . Intermediate mixtures ($V_{rubber} = 0.4$ and 0.5) exhibit consistent behavior at all stress levels, and there is no transition from rubber-like to sand-like response with increasing confinement. However, the rubber particles are squeezed, the mean stress in the sand increases around the equatorial plane of the rubber particles (arching in the vertical direction plus increased lateral confinement associated to rubber incompressibility), and the shear wave velocity is highest for $V_{rubber} = 0.1$ to 0.2 (Figs. 12 and 15).

Fig. 15. Numerical simulation of shear wave propagation in $V_{\text{rubber}} = 0.2$ sand–rubber mixture. Time series. The vertical straight line indicates the travel time in a homogeneous medium. (a) $V_s(\text{sand}) = \text{constant}$. (b) $V_s(\text{sand}) = \alpha(\sigma'/\text{kPa})^\beta$.

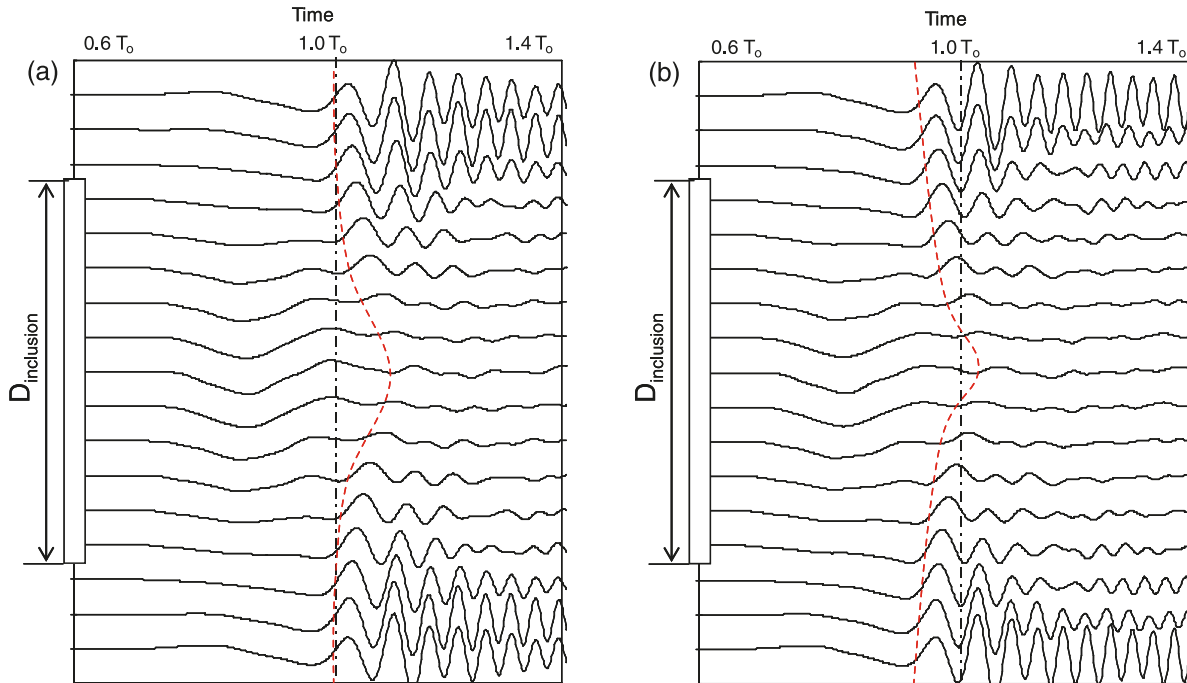
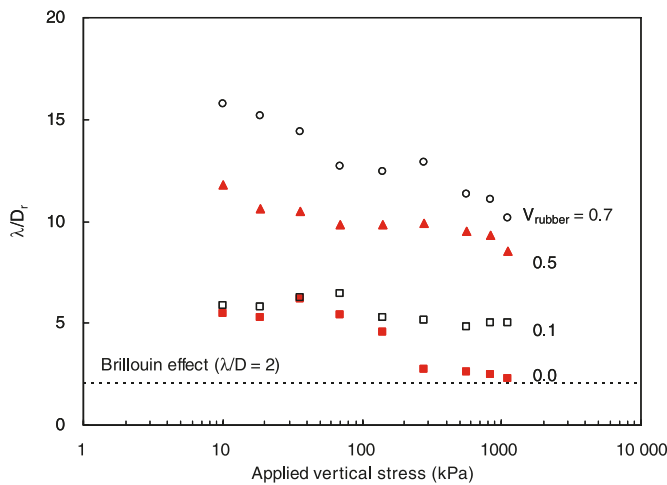


Fig. 16. Wavelength of received shear waves normalized by the diameter of large rubber particles versus applied vertical stress.



Summary and conclusions

Experimental and numerical results for mixtures made of small sand grains and large rubber chips ($D_r/D_s \approx 10$) show the following:

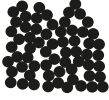


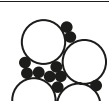
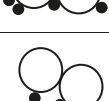
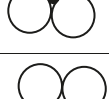

- (1) The high contrast in particle size, shape, and mass density in typical sand–rubber mixtures causes segregation, particularly when the volume fraction of rubber particles exceeds $V_{\text{rubber}} > 0.7$.
- (2) The sand skeleton controls the behavior for $V_{\text{rubber}} < 0.3$, while the rubber skeleton prevails at $V_{\text{rubber}} \geq 0.6$. For intermediate mixtures, large rubber particles tend to be

squeezed at high confinement and fill the interfacial voids; no significant increase in sand-to-sand coordination is anticipated.

- (3) The quasi-static compressibility in all mixtures is a power function of the effective stress.
- (4) The effective stiffness of random binary mixtures of linear elastic continua decreases monotonically with volume fraction of the soft material. This is not the case in binary mixtures of soft and stiff granular materials. The constrained modulus is highest in the pure sand specimen (i.e., $V_{\text{rubber}} = 0$), and experiences little change for $V_{\text{rubber}} = 0.1$ and 0.2 . On the other hand, short wavelength propagation ($\lambda/D_r \approx 2\sim 10$) shows higher propagation velocity in mixtures with $V_{\text{rubber}} = 0.1$ and 0.2 than in the pure sand specimen. This phenomenon is the result of high mean-stress in the sand around the equatorial plane of soft particles due to soil arching around the deformable rubber particles (increasing vertical stress) and incompressible rubber deformation (increasing horizontal stress).
- (5) High frequency wave propagation may bias the interpretation of the small-strain quasi-static stiffness in heterogeneous sand–rubber mixtures. Therefore, the relative size between wavelength and internal scale must be considered in data interpretation.

These observations provide the foundations for optimal engineering design of heterogeneous granular materials made of stiff and soft particles, such as mineral aggregates mixed with recycled tire chips. Both numerical and experimental results show that the mechanical response of sand–rubber mixtures depends on (i) the volume fraction of rubber V_{rubber} and (ii) the relative grain size D_r/D_s . In particular, there are clear differences in fabric, particle-level mechanisms, and macroscale behavior between sand–rubber mix-

Fig. 17. Schematic summary of rubber–sand interaction in mixtures with different particle size ratios.

Fabric and volume fraction	Previous results in Lee et al. (2007): $D_r \ll D_s$ (consider small filled circles as rubber grains)	This study: $D_r \gg D_s$ (consider large empty circles as rubber grains)
	$V_{rubber} = 1.0$: Soft rubber skeleton	$V_{rubber} = 0$: Stiff sand skeleton
	$V_{rubber} > 0.6$: Rubber controlled stiffness	$0 < V_{rubber} < 0.2$ Increased stiffness outside rubber mid-plane due to arching and rubber incompressibility
	$V_{rubber} \sim 0.4$: Minimum porosity "Transition mixture" Rubber separates sand at low σ' Sand contacts form at high σ'	$V_{rubber} \sim 0.4$: Sand forms percolating skeleton There is rubber–rubber interaction
	$0 < V_{rubber} < 0.3$ Rubber prevents buckling of sand columns Segregation (if rubber can run through pores)	$V_{rubber} \sim 0.6$: Minimum porosity
	$0 < V_{rubber} < 0.3$ Rubber prevents buckling of sand columns Segregation (if rubber can run through pores)	$0.7 < V_{rubber} < 1.0$ Segregation (if sand can run through pores)
	$V_{rubber} < 0.2$: Rubber: small effect on stiffness	$V_{rubber} > 0.8$: Sand has a small effect on stiffness
	$V_{rubber} = 0$: Stiff sand skeleton	$V_{rubber} = 1.0$: Soft rubber skeleton

tures made with small rubber particles ($D_r/D_s \ll 1$) and those made with large rubber particles ($D_r/D_s \gg 1$).

Acknowledgements

This research is supported by a grant on Scale Effects in Soils from the National Science Foundation and by the Goizueta Foundation.

References

Ahmed, I., and Lovell, C.W. 1993. Rubber soils as lightweight geomaterials. *In* Lightweight artificial and waste materials for embankments over soft soils. Transportation Research Record 1422. National Academy Press, Wash. pp. 61–70.

ASTM. 2006. Standard test methods for specific gravity of soil solids by water pycnometer. ASTM standard D854-06. American Society for Testing and Materials, West Conshohocken, Pa.

Bosscher, P.J., Edil, T.B., and Kuraoka, S. 1997. Design of highway embankments using tire chips. *Journal of Geotechnical and Geoenvironmental Engineering*, **123**(4): 295–304. doi:10.1061/(ASCE)1090-0241(1997)123:4(295).

Edil, T.B., and Bosscher, P.J. 1994. Engineering properties of tire chips and soil mixtures. *Geotechnical Testing Journal*, **17**: 453–464.

Feng, Z.Y., and Sutter, K.G. 2000. Dynamic properties of granulated rubber and mixtures. *Geotechnical Testing Journal*, **23**: 338–344.

Foose, G.J., Benson, C.H., and Bosscher, P.J. 1996. Sand reinforced with shredded waste tires. *Journal of Geotechnical Engineering*, **122**(9): 760–767. doi:10.1061/(ASCE)0733-9410(1996)122:9(760).

Garga, V.K., and O’Shaughnessy, V. 2000. Tire-reinforced earth-fill. Part I: Construction of a test fill, performance, and retaining wall design. *Canadian Geotechnical Journal*, **37**(1): 75–96. doi:10.1139/cgj-37-1-75.

Gebhardt, M.A. 1997. Shear strength of shredded tires as applied to the design and construction of a shredded tire stream crossing. M.Sc. thesis, Iowa State University, Ames, Iowa.

German, R.M. 1989. Particle packing characteristics. Metal Powder Industries Federation, Princeton, N.J. 443p.

Ghazavi, M. 2004. Shear strength characteristics of sand-mixed with granular rubber. *Geotechnical and Geological Engineering*, **22**: 401–416. doi:10.1023/B:GEGE.0000025035.74092.6c.

Guyon, E., Oger, L., and Plona, T.J. 1987. Transport properties in sintered porous media composed of two particles sizes. *Journal of Applied Physics D. Applied Physics (Berlin)*, **20**: 1637–1644.

Hardin, B.O., and Black, W.L. 1968. Vibration modulus of normally consolidated clay. *Journal of the Soil Mechanics and Foundations Division, ASCE*, **89**: 353–369.

Heimdahl, C., and Druscher, A. 1999. Elastic anisotropy of tire shreds. *Journal of Geotechnical and Geoenvironmental Engineering*, **125**(5): 383–389. doi:10.1061/(ASCE)1090-0241(1999)125:5(383).

Humphrey, D.N., and Manion, W. 1992. Properties of tire chips for lightweight fill. *In* Grouting, soil improvement, and geosynthetics, ASCE. Edited by R.H. Borden, R.D. Holtz, and I. Juran. Geotechnical Special Publication 30, pp. 1344–1355.

Humphrey, D.N., Sandford, T.C., Cribbs, M.M., and Manion, W.P. 1993. Shear strength and compressibility of tire chips for use as retaining wall backfill. *In* Lightweight artificial and waste materials for embankments over soft soils. Transportation Research Record 1422. National Academy Press, Wash. pp. 29–35.

- Knox, D.P., Stokoe, K.H., and Kopperman, S.E. 1982. Effect of state of stress on velocity of low-amplitude shear waves propagating along principal stress directions in dry sand. Report GR 82-23. Civil Engineering Department, University of Texas, Austin, Tex.
- Lee, J.H., Salgado, R., Bernal, A., and Lovell, C.W. 1999. Shredded tires and rubber-sand as lightweight backfill. *Journal of Geotechnical and Geoenvironmental Engineering*, **125**(2): 132-141. doi:10.1061/(ASCE)1090-0241(1999)125:2(132).
- Lee, J.S., Dodds, J., and Santamarina, J.C. 2007. Behavior of rigid-soft particle mixtures. *Journal of Materials in Civil Engineering*, **19**(2): 179-184. doi:10.1061/(ASCE)0899-1561(2007)19:2(179).
- Masad, E., Taha, R., Ho, C., and Papagionnakis, T. 1996. Engineering properties of tire/rubber mixtures as a lightweight fill material. *Geotechnical Testing Journal*, **19**: 297-304.
- Mavko, G.M., Mukerji, T., and Dvorkin, J. 1998. *The rock physics handbook*. Cambridge University Press, New York. 329 pp.
- Nagasaka, Y., Horiuchi, S., and Higaki, K. 1996. Status on utilization and disposal of industrial waste in Japan. *In Environmental geotechnics*. Edited by M. Kamon. A.A. Balkema, Rotterdam. pp. 839-844.
- Nightingale, D.E.B., and Green, W.P. 1997. An unsolved riddle: tire chips, two roadbeds, and spontaneous reactions. *In Testing soil mixed with waste or recycled materials*. Edited by M.A. Wasemiller and K.B. Hoddinott. ASTM STP 1275, pp. 265-285.
- Pamukcu, S., and Akbulut, S. 2006. Thermoelastic enhancement of damping of sand using synthetic ground rubber. *Journal of Geotechnical and Geoenvironmental Engineering*, **132**(4): 501-510. doi:10.1061/(ASCE)1090-0241(2006)132:4(501).
- Potts, B.D., and Santamarina, J.C. 1993. Geotechnical tomography: the effects of diffraction. *Geotechnical Testing Journal*, **16**: 510-517.
- Rubber Manufacturers Association. 2006. Scrap tire markets in the United States. 90 pp. Available from www.rma.org.
- Santamarina, J.C., Klein, K.A., and Fam, M.A. 2001. *Soils and waves*. John Wiley & Sons, New York.
- Tatliso, N., Benson, C.H., and Edil, T.B. 1997. Effect of fines on mechanical properties of soil-tire chip mixtures. *In Testing soil mixed with waste or recycled materials*. Edited by M.A. Wasemiller and K.B. Hoddinott. ASTM STP 1275. pp. 93-108.
- Walter, J.D., and Clark, S.K. 1981. Cord reinforced rubber. *In Mechanics of pneumatic tires*. Edited by S.K. Clark. U.S. Department of Transportation, National Highway Traffic Safety Administration, Wash.
- Wielandt, E. 1987. On the validity of ray approximation for interpreting delay times. *In Seismic tomography*. Edited by G.D. Nolet. Reidel publishing Co., Boston, Mass. pp. 85-98.
- Wu, W.Y., Benda, C.C., and Cauley, R.F. 1997. Triaxial determination of shear strength of tire chips. *Journal of Geotechnical and Geoenvironmental Engineering*, **123**(5): 479-482. doi:10.1061/(ASCE)1090-0241(1997)123:5(479).
- Yanagida, T., Matchett, A.J., and Coulthard, J.M. 2002. Damping and elastic properties of binary powder mixtures. *Powder Technology*, **127**: 107-115. doi:10.1016/S0032-5910(02)00113-4.
- Yang, S., Lohnes, R.A., and Kjartanson, B.H. 2002. Mechanical properties of shredded tires. *Geotechnical Testing Journal*, **25**(1): 44-52.
- Youd, T.L. 1973. Factors controlling the maximum and minimum densities of sands. *In Evaluation of relative density and its role in geotechnical projects involving cohesionless soils*. Edited by E.T. Selig and R.S. Ladd. ASTM Special Technical Publication 523. American Society for Testing and Materials, Philadelphia, Pa. pp. 98-112.
- Youwai, S., and Bergado, D.T. 2003. Strength and deformation characteristics of shredded rubber tire - sand mixtures. *Canadian Geotechnical Journal*, **40**(2): 254-264. doi:10.1139/t02-104.
- Zheng-Yi, F., and Sutter, K.G. 2000. Dynamic properties of granulated rubber/sand mixtures. *Geotechnical Testing Journal*, **23**(3): 338-344.
- Zornberg, J.G., Cabral, A.R., and Viratjandr, C. 2004. Behaviour of tire shred - sand mixtures. *Canadian Geotechnical Journal*, **41**(2): 227-241. doi:10.1139/t03-086.

Copyright of *Canadian Geotechnical Journal* is the property of NRC Research Press and its content may not be copied or emailed to multiple sites or posted to a listserv without the copyright holder's express written permission. However, users may print, download, or email articles for individual use.